Supplementary Information

for

The use of energy looping between Tm^{3+} and Er^{3+} ions to obtain an intense upconversion under the 1208 nm radiation and its use in temperature sensing

Tomasz Grzyb[1]*, Inocencio R. Martín[2], Radian Popescu[3]

[1]*Department of Rare Earths, Faculty of Chemistry, Adam Mickiewicz University in Poznań, Uniwersytetu Poznańskiego 8, 61-614 Poznań, Poland*

[2]*Departamento de Fisica, Universidad de La Laguna, Instituto de Materiales y Nanotecnología, 38200 San Cristóbal de La Laguna, Santa Cruz de Tenerife, Spain*

[3]*Laboratory for Electron Microscopy, Karlsruhe Institute of Technology, Engesserstrasse 7, 76131 Karlsruhe, Germany*

**E-mail: tgrzyb@amu.edu.pl*

1. Experimental

1.1. Synthesis of rare earth acetates

To synthesise 10 mmol of each rare earth acetate, 5 mmol of rare earth oxide was dissolved in 40 ml of a 40% acetic acid solution. The solution was heated in the three-neck flask at 85°C under a reflux condenser at atmospheric pressure. After 16 h, the mixture was cooled to room temperature under the flow of pure nitrogen. Unreacted acid from filtered solution was removed using a rotary evaporator at 50°C, with a vacuum of around 50 mbar, to near dryness (for around 1 h). The obtained wet solid material was dissolved in an 80% acetic acid solution. For each 1 mmol of rare earth oxide, 1.1–1.4 ml of acetic acid solution was used, and the volume of solution depended on the type of rare earth acetate. The solution was put into a three-neck flask connected to a reflux condenser and heated to 85°C under a nitrogen atmosphere. Then, acetic acid (≥99%) was added to the solution by funnel during cooling (dropped acetic acid volume was the same as the heated aqueous rare earth acetic acid solution). The solution was finally heated under a nitrogen atmosphere at 120°C for 2 h. Then, the solution was cooled to room temperature, and the powder material was obtained after the evaporation of unreacted acid using a rotary evaporator at 50°C (around 25 mbar) for around 4 h. The amount of physically adsorbed water was estimated using thermogravimetric analysis (TGA).

1.2. Synthesis conditions

Nanoparticle (NP) syntheses were conducted utilising a Schlenk line. When applying low pressure in the synthesis process, the pressure within the line was consistently measured to be $<10^{-1}$ mbar. Reagents were consistently introduced into the solution of oleic acid and octadecene under a nitrogen flow, followed by consistent outgassing of the system until reaching a low pressure. The reaction heating rate was consistently set at 5°C per minute. Precipitation of the obtained NPs was achieved using a rotary centrifuge operating at 9000 rpm for 3 minutes. For precipitation, ethanol was consistently added to the mixture in a volume ratio of 1 ml of n-hexane to 1 ml of ethanol. When referring to the dissolution of NPs in n-hexane, it indicates the addition of 5 ml of n-hexane per 1 mmol of NPs.

2. Structure and morphology

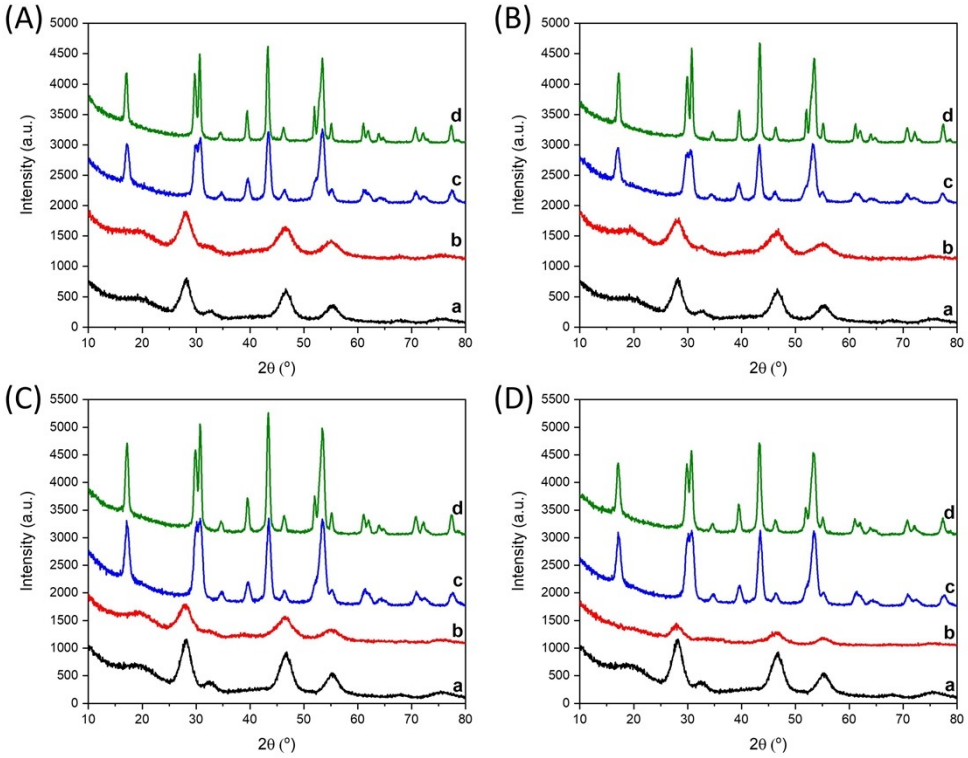

Fig. S1. XRD patterns performed for: (A) a shell α-$NaYF_4$; b) core α-$NaYF_4$:2%Tm^{3+}; c) core β-$NaYF_4$:2%Tm^{3+}; d) core@shell β-$NaYF_4$:2%Tm^{3+}@β-$NaYF_4$; (B) a) shell α-$NaYF_4$; b) core α-$NaYF_4$:5%Er^{3+},2%Tm^{3+}; c) core β-$NaYF_4$:5%Er^{3+},2%Tm^{3+}; d) core@shell β-$NaYF_4$:5%Er^{3+},2%Tm^{3+}@β-$NaYF_4$; (C) a) shell α-$NaYF_4$; b) core α-$NaYF_4$:2%Er^{3+},2%Tm^{3+}; c) core β-$NaYF_4$:2%Er^{3+},2%Tm^{3+}; d) core@shell β-$NaYF_4$:2%Er^{3+},2%Tm^{3+}@β-$NaYF_4$; (D) a) shell α-$NaYF_4$; b) core α-$NaYF_4$:2%Er^{3+},5%Tm^{3+}; c) core β-$NaYF_4$:2%Er^{3+},5%Tm^{3+}; d) core@shell β-$NaYF_4$:2%Er^{3+},5%Tm^{3+}@β-$NaYF_4$.

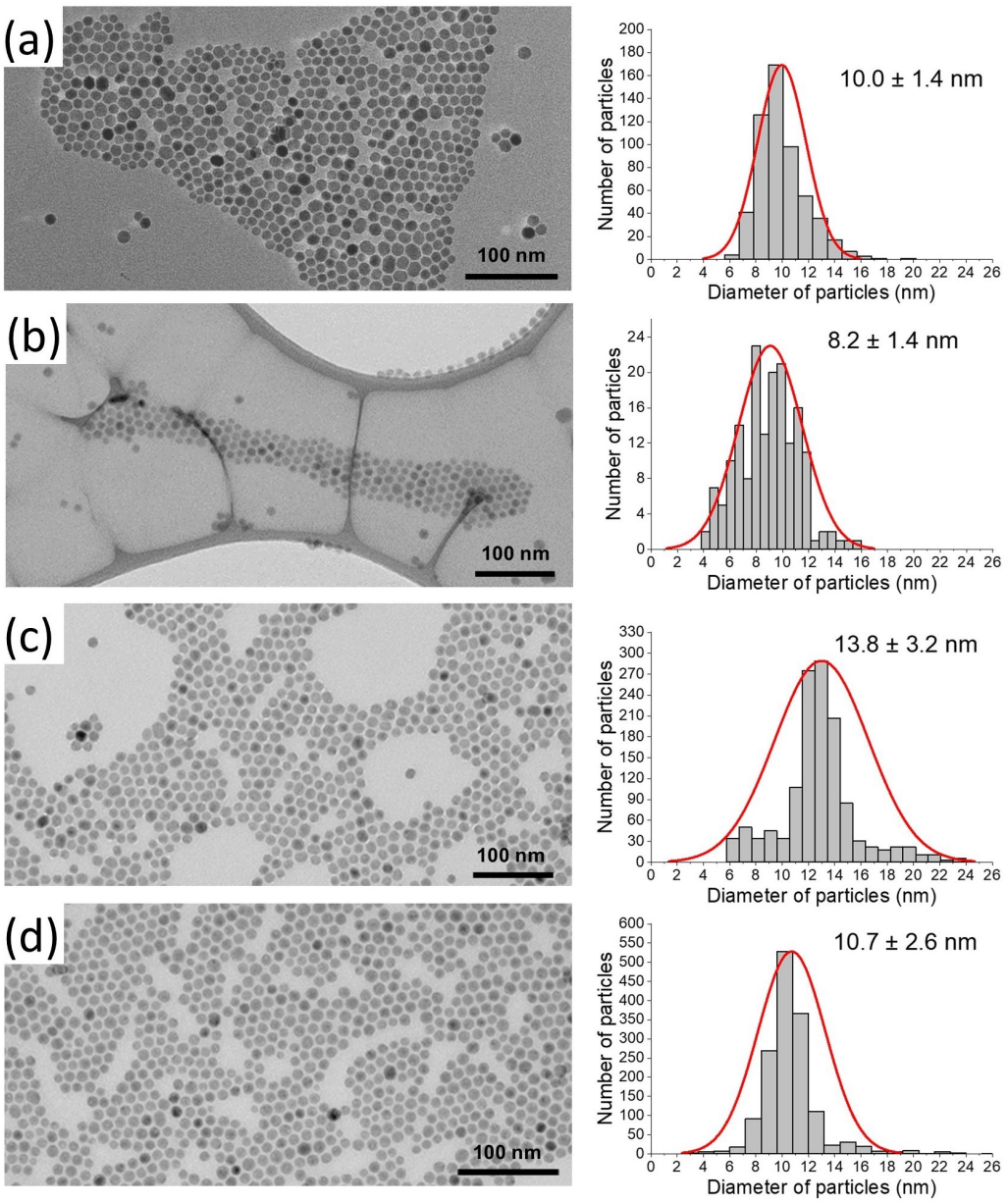

Fig. S2. TEM images recorded for: (a) β-$NaYF_4$:2%Tm^{3+}; (b) β-$NaYF_4$:5%Er^{3+},2%Tm^{3+}; (c) β-$NaYF_4$:2%Er^{3+},2%Tm^{3+}; and (d) β-$NaYF_4$:2%Er^{3+},5%Tm^{3+}.

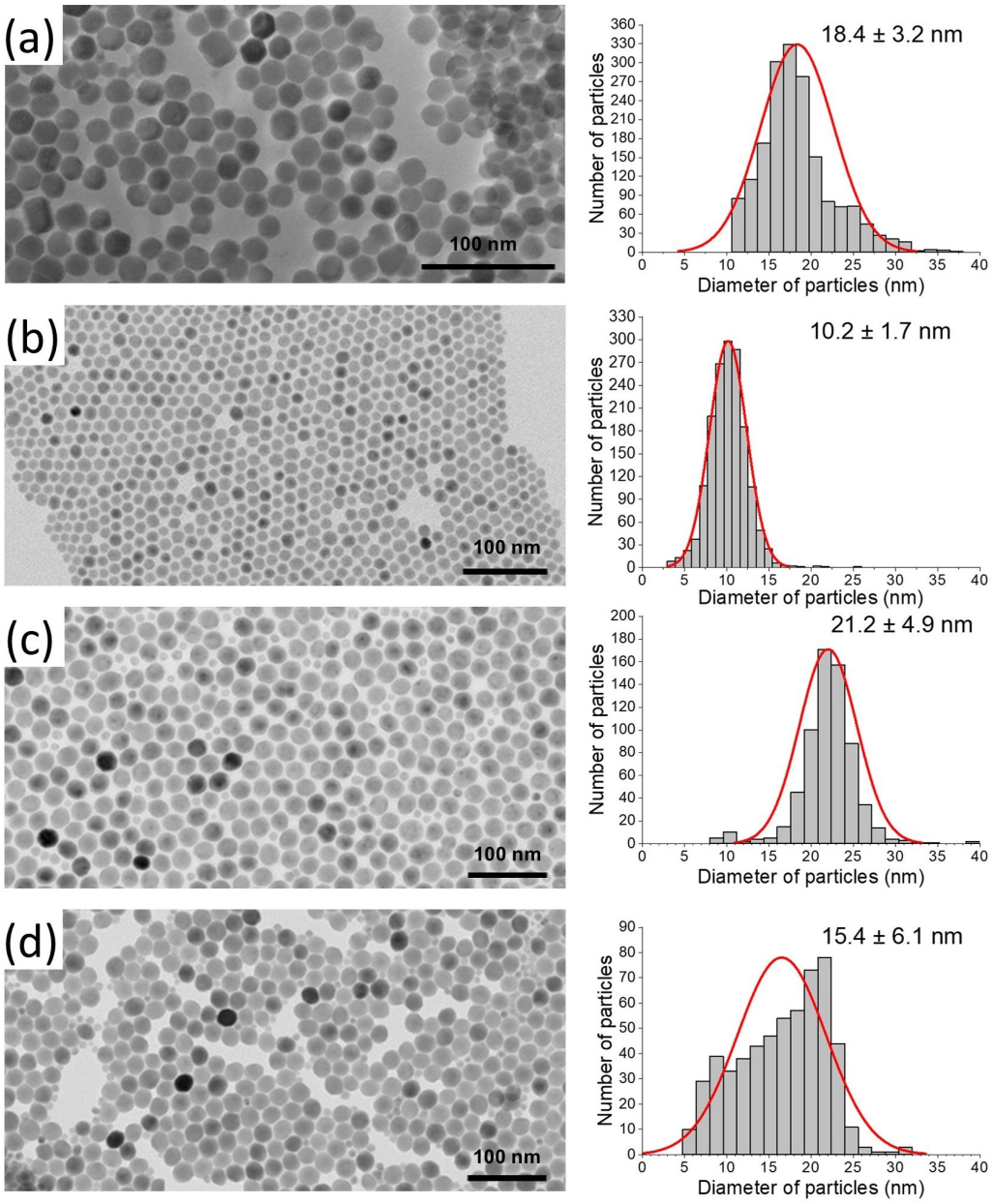

Fig. S3 TEM images recorded for: (a) β-$NaYF_4$:2%Tm^{3+}@β-$NaYF_4$; (b) β-$NaYF_4$:5%Er^{3+},2%Tm^{3+}@β-$NaYF_4$; (c) β-$NaYF_4$:2%Er^{3+},2%Tm^{3+}@β-$NaYF_4$; and (d) β-$NaYF_4$:2%Er^{3+},5%Tm^{3+}@β-$NaYF_4$.

3. Spectroscopic properties

The number of photons required to populate the emitting levels of Tm^{3+} and Er^{3+} ions can be obtained from the following relation:[1]

$$I_{UC} \propto P^n \tag{1}$$

where I_{UC} is the up-conversion emission intensity, P is the pump laser power density, and n is the number of photons required. The slope values of dependency of the upconversion intensity on the laser power density drawn in a diagram with a double-logarithmic scale represent n, i.e., the number of photons. The dependencies recorded for the studied NPs are presented in Fig. 3.

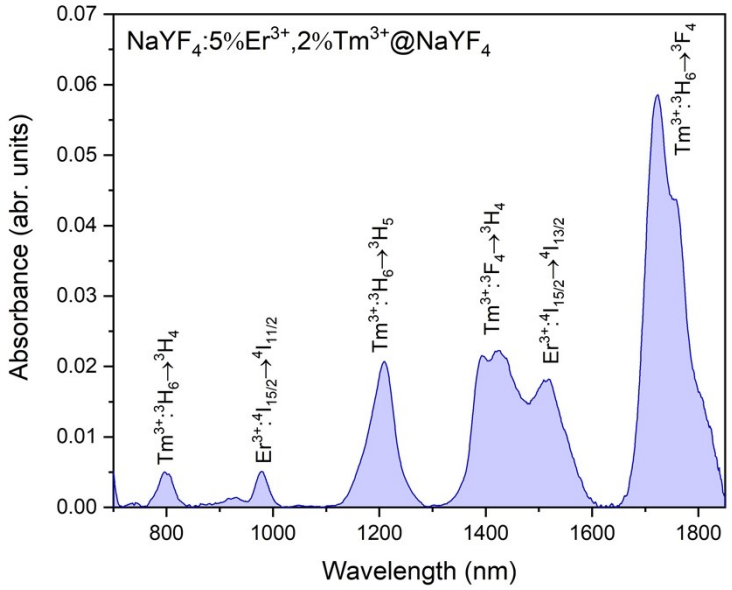

Fig. S4. Absorption spectra measured for $NaYF_4$:2%Tm^{3+},5%Er^{3+}@$NaYF_4$ NPs.

The Kohlrausch function was applied to calculate emission rise times presented in Figs. S5 and S6.[2–4] This function can be used for kinetics deviating from exponential. In the case of the studied samples, fitting with single- or bi-exponential functions was impossible due to unsatisfactory results. The Kohlrausch function can be described as:

$$I(t) = exp\left[-\left(\frac{t}{\tau_r}\right)^{\beta}\right] \quad (2)$$

where β is the nonexponentiality degree and τ_r is the decay time of the Kohlrausch function. This function can be used for the calculation of rise and decay times.[5]

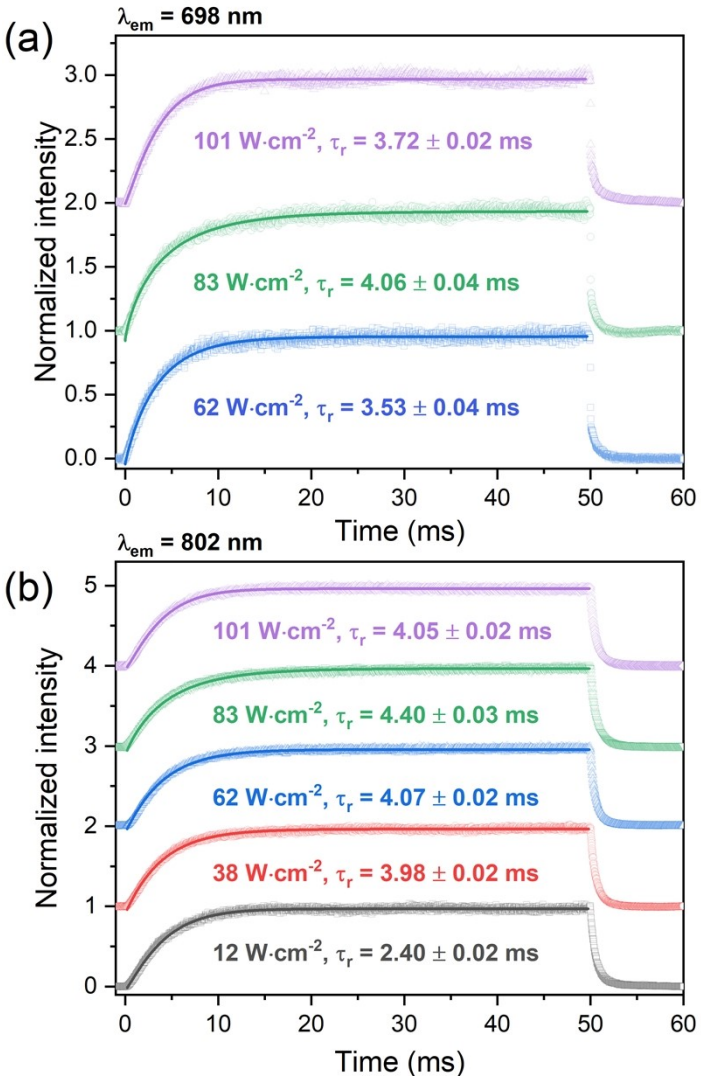

Fig. S5. Evolution of emission under 1208 nm excitation measured for $NaYF_4$:2%Tm^{3+}@$NaYF_4$ NPs at (a) 698 nm and (b) 802 nm. The rise rimes, τ_r were calculated by the Kohlrausch function.

Upconversion mechanism for the $^3F_3$ level

The upconversion curve obtained detecting the $^3F_3$ does not show a short rise, indicating that the ESA mechanism is not predominant. Therefore, two different mechanisms can be considered to populate this level under excitation at the $^3H_5$ level with 1208 nm laser light. The first mechanism consists of the participation of two excited ions in their $^3H_5$ levels and energy transfer between them. The second mechanism consists of relaxation from the $^3H_5$ level to the $^3F_4$ level (with a long lifetime) and energy transfer between Tm^{3+} ions at this level and the other Tm^{3+} ion excited in the $^3H_5$ level. Both mechanisms have been analysed using rate equations similar to the upconversion processes studied in the article published previously.[6] As shown in Fig. S6, the upconversion emission obtained at 698 nm agrees with an energy transfer between the $^3H_5$ and $^3F_4$ levels.

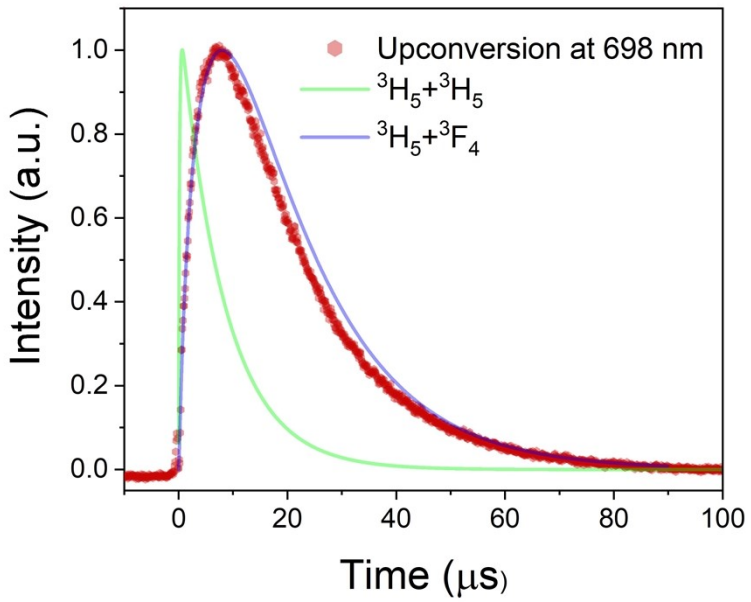

Fig. S6. Upconversion temporal dependence at 698 nm obtained under excitation at 1208 nm and temporal dynamics simulation assuming different upconversion processes.

The emission observed at 802 nm originating from the $^3H_4$ level may stem from various upconversion mechanisms. However, when considering relaxation from the $^3F_3$ level, its population can be described as follows:

$$\frac{d^3H_4(t)}{dt} = -\frac{^3H_4(t)}{\tau_4} + W_{NR}{}^3F_3(t) \quad (3)$$

where τ_4 is the intrinsic lifetime of the $^3H_4$ level, and W_{NR} is the non-radiative relaxation probability from the $^3F_3$ level. Subsequently, the temporal evolution of the $^3H_4$ level can be derived from Eq. (3) while considering the temporal dynamics of $F_3(t)$ as illustrated in Fig. S6.

As shown in Fig. S7, the comparison between the experimental upconversion at 802 nm and the temporal dynamics simulation obtained from Eq. (3) are very similar, indicating that the $^3H_4$ level is populated from the $^3F_3$ level.

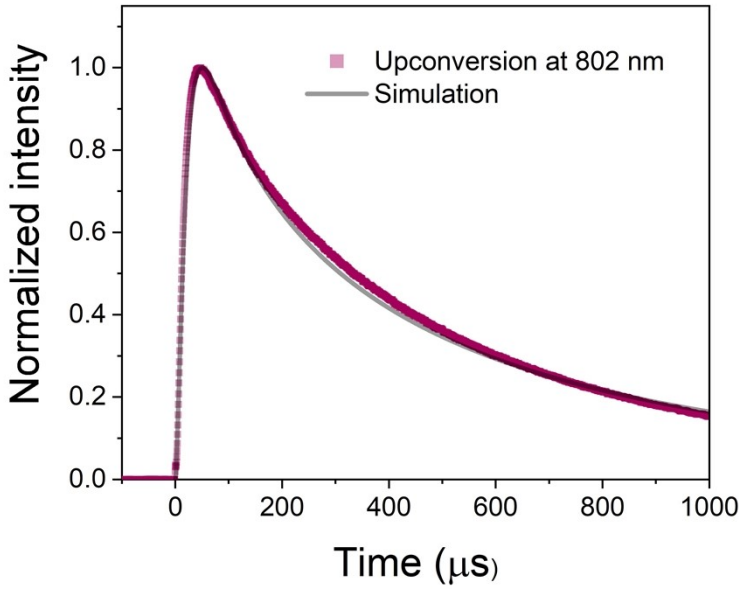

Fig. S7. Upconversion temporal dependence at 802 nm obtained under excitation at 1208 nm, and simulation obtained a population from the $^3F_3$ level.

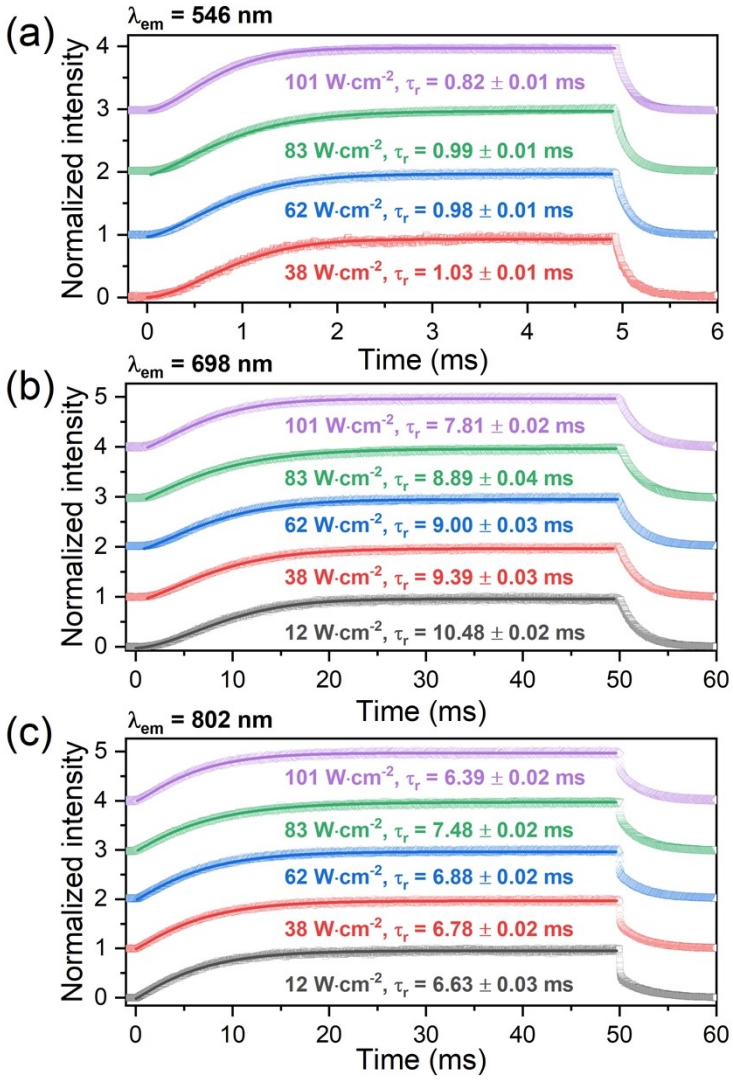

Fig. S8. Evolution of emission under 1208 nm excitation measured for $NaYF_4$:5%Tm^{3+},2%Er^{3+}@$NaYF_4$ NPs at (a) 546 nm, (b) 698 nm and (c) 802 nm. The Kohlrausch function calculated the rise rimes, τ_r.

4. Temperature sensing properties

To calculate luminescence intensity ratios (LIRs) presented in Fig. 6a, emission peaks were integrated using Origin Pro 2022. Next, the dependencies of LIRs on temperature were fitted with two types of functions. As the $^2H_{11/2}$ and $^4S_{3/2}$ excited states of Er^{3+} ions are thermally coupled, the dependence of 526/546 nm LIR on temperature was fitted with Boltzmann-type function:

$$LIR \equiv \frac{I_{526}}{I_{546}} = B \times exp\left(-\frac{\Delta E}{k_B T}\right) \quad (4)$$

where LIR is the luminescence intensity ratio of the emission bands, k_B is the Boltzmann constant, ΔE is the energy separation between the barycenters of the I_{528} and I_{546} bands, T is the absolute temperature, and B is a constant.

The remaining LIRs: 660/698 nm, 982/698 nm, 982/660 nm and 982/802 nm were fitted using a cubic function, giving a better fit than the Boltzmann-type function (Eq. 4).

$$LIR \equiv \frac{I_1}{I_2} = A + B \times T + C \times T^2 + D \times T^3 \quad (5)$$

where LIR is the luminescence intensity ratio of the two I_1 and I_2 s mission bands, T is the absolute temperature, and A, B and C are constants. The obtained R^2 correlation coefficients were not lower than 0.99.

The relative sensitivities, $S_r$were calculated using Eq. 5. The calculated values were plotted in Fig. 6d. The S_r value (%/°C^{-1}) presents how the measured LIR used for optical temperature sensing changes per 1 °C of temperature:

$$S_r = 100\% \times \frac{1}{LIR} \times \frac{dLIR}{dT} \quad (6)$$

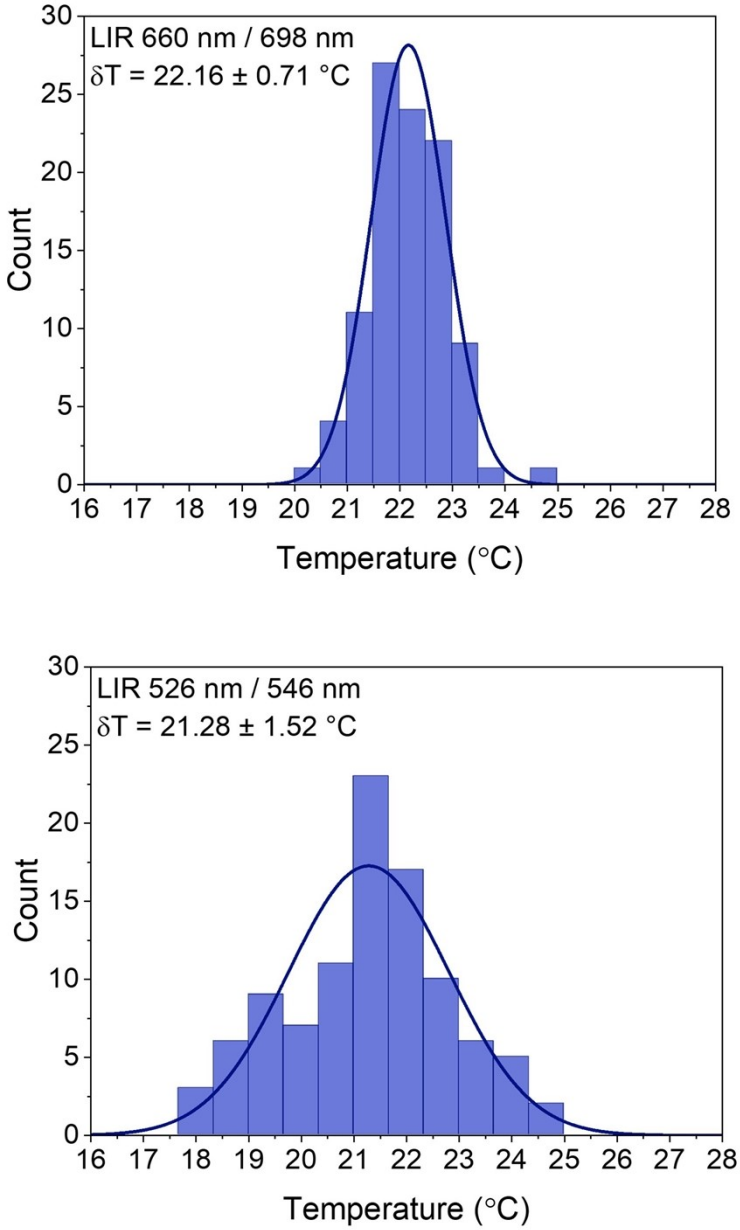

Fig. S9. Temperature resolution determined from 100 emission measurements at room temperature for $NaYF_4$:2%Er^{3+},5%Tm^{3+}@$NaYF_4$ NPs under λ_{ex} = 1208 nm excitation.